Supporting Information

Gap Size-Dependent Plasmonic Enhancement in Electroluminescent Tunnel Junctions

Angela L. Paoletta,† E-Dean Fung,‡ and Latha Venkataraman*,†,‡

†Department of Chemistry and ‡Department of Applied Physics and Applied Mathematics, Columbia University, New York, New York 10027, United States

*Email: lv2117@columbia.edu

Contents:

S1. Custom STM-BJ Technique

Figure S1 shows a full conductance and photovoltage trace, measured simultaneously. The measured bias and piezo position are also shown. The electrodes are in contact at the start of each trace and are pulled apart at a bias of 200 mV. Next, the electrodes are held briefly as the bias is ramped up to 1.65 V. The electrodes are pushed together at this high bias (gray shaded region) and elevated conductance and photovoltage is seen in this region. The bias drops upon reformation of the contact as we have a resistor in series with the junction over which most of the voltage drops. Finally, the electrodes are pulled apart again at 200 mV to reset the experiment.

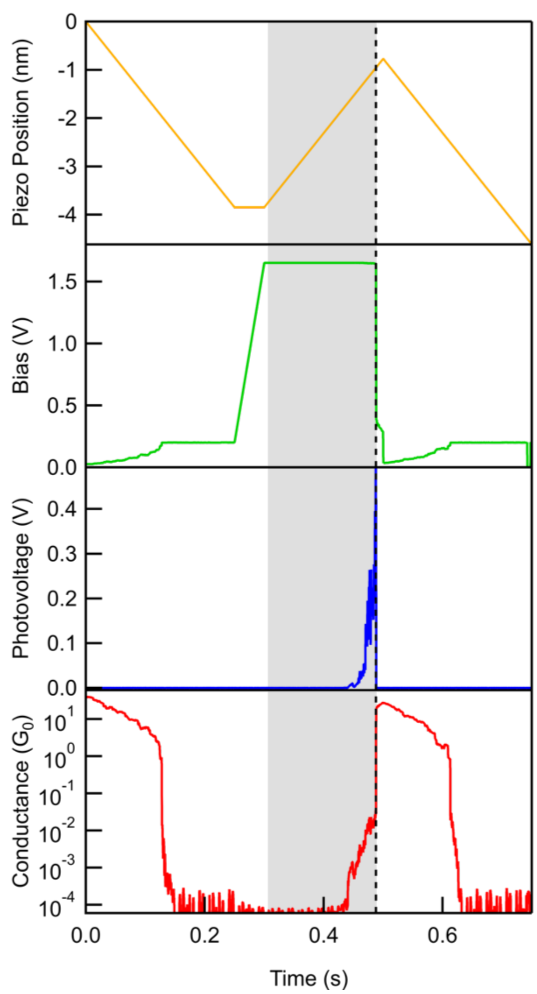

Figure S1. Full trace showing piezo position, measured bias, photovoltage, and conductance. The region of interest for tunnel junction formation is shaded gray.

S2. Snap into Contact and Estimation of Gap Size

We note that the distance relative to contact is less than the actual gap size due to a snap into contact. The actual gap size is the distance from a contact exceeding $1G_0$ plus the distance between the electrodes when the snap into contact occurs. We have also observed that there is a larger snap into contact for higher biases. In other words, the snap occurs at lower conductances and the gap size is underestimated by a larger amount. This is due to increased force due to larger charge separation. There is thus a larger difference between the distance relative to contact and the actual gap size for higher biases compared to lower biases.

S3. Coulomb Blockade Model

Our model, which is based on the models developed by Tosbiska et al.[1] and Xu et al.,[2] is described fully in the Supplementary Information of our previous work.[3] In this previous work, the model is also compared numerically to the Xu model and multielectron processes are considered.

Here, we summarize the model for one-electron processes. For these processes, the probability of emitting a photon of energy within the interval [E, E + dE] is $P_{1e}(E)$ or the probability density of emission. $P_{1e}(E)$ is total emission probability, not per electron. It has units of inverse energy, eV^{-1} and can be defined as:

$$P_{1e}(E) = G_0\widetilde{D}(E)\tilde{S}(E)$$

In contrast to the main text, the tildes over D(E) and S(E) indicate the non-normalized versions, defined as:

$$\widetilde{D}(E) = \frac{\left|\tilde{Z}(E)\right|^2}{E^2}$$

$$\tilde{S}(E) = G_0 \sum_n \left[2\tau_n^2 B(E) + \tau_n(1 - \tau_n)\sum_{\pm} B(E \pm eV)\right]$$

The complex impedance of the electromagnetic environment is denotated $\tilde{Z}$(E) and is modelled by an RLC circuit, as described by others.[1,2] We model this as a single bias-dependent plasmon mode with a resonance centered at 1.65 eV or 750 nm:

$$\tilde{Z}_\omega = i\sqrt{\frac{L}{C}}\frac{\omega_0\omega}{\omega_0^2 - \omega^2 + i\omega\eta} \qquad \omega_0 = \frac{1}{\sqrt{LC}} \qquad \eta = RC$$

$$\frac{Z(E)}{E} = \frac{G_0\tilde{Z}(E)}{E} = i\frac{\hbar G_0}{C}\frac{1}{(\hbar\omega_0)^2 - E^2 + iE\hbar\eta}$$

We use C = 0.1 a$F, \hbar\eta$ = 0.5 eV, and $\hbar\omega_0$ = 1.65 eV to reproduced spectra similar to our experimental spectra. $\tilde{Z}$(E) can be normalized to G_0, i.e. $Z(E) \equiv G_0\tilde{Z}(E)$, which can then be used to normalize $\tilde{D}(E)$, giving the normalized D(E), defined as:

$$D(E) = \frac{|Z(E)|^2}{E^2} = \frac{G_0^2|\tilde{Z}(E)|^2}{E^2} = G_0^2\tilde{D}(E)$$

We also multiply $\tilde{S}$(E) by G_0 to obtain the normalized version S(E), and arrive at the definition of the probability density of emission stated in the main text:

$$P_{1e}(E) = D(E)S(E)$$

Our model does not include the additional prefactor of $\frac{|\mathcal{T}|^2}{h}\alpha^2$ from the Tobiska[1] and Xu[2] models. These researchers use a two-state quantum dot as a detector and the prefactor accounts for the coupling between the two states of a quantum dot, $\mathcal{T}$, and the dimensionless coupling between the RLC circuit and the detector, α. In our work here, we correct the experimental spectrum for the wavelength-dependent responsivity of our detector (a silicon photomultiplier, abbreviated SiPM). Thus, we wish to obtain a calculated spectrum that does not account for changes in detector sensitivity. We note that in our previous work,[3] we include a prefactor Q(E) in our model to account for the detector in the calculated spectrum. This is because the experimental spectra are not corrected for detector response in that work.

S4. Increasing Photoefficiency is Wavelength-Dependent

In Figure S2, we show that the wavelength dependence seen in the photoefficiency slope histograms of Figure 3b-e can also be seen in the corresponding two-dimensional photoefficiency versus distance histograms. For a bias of 1.65 V, the light close to 850 nm shows the greatest increase in photoefficiency as the gap closes.

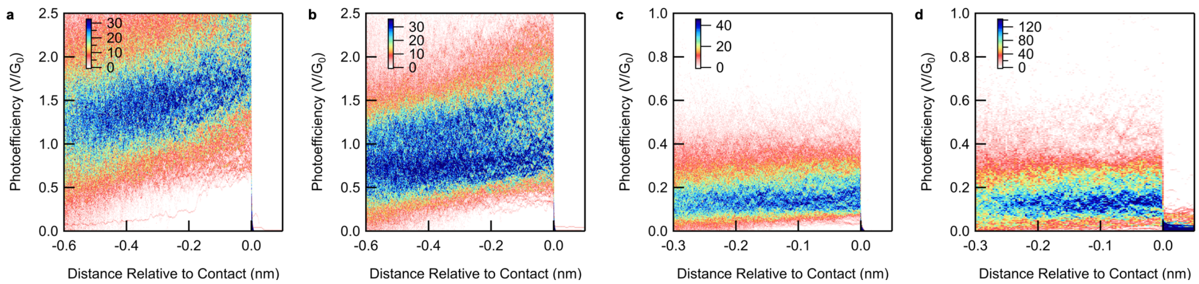

Figure S2. Two-dimensional histogram of photoefficiency versus distance relative to contact formation for light emission of wavelengths (a) 850 nm and longer, (b) 750 to 850 nm, (c) 750 nm and shorter, and (d) 650 nm and shorter. These histograms correspond to the photoefficiency slope histograms in Figure 3b-e.

We also show photoefficiency slope histograms for various bandpass filters with a FWHM (full width at half maximum) of 10 nm (Figure S3). When measuring only light around 800 or 850 nm, the majority of junctions show increasing photoefficiency with decreasing gap size, as shown in Figures S3 and S4. We see that the gap size dependence diminishes for wavelengths farther from this LSPR peak (Figure S3a,d,e).

Due to the spectrum of light emitted and the wavelength-dependent responsivity of the SiPM, the photoefficiency's signal to noise ratio is not high enough to determine a slope for the majority of traces for the 1000, 700, and 650 nm bandpass filters. Histograms for these wavelengths would be skewed by only representing the junctions that give the highest photovoltage and thus the highest signal to noise. For this minority selection, we see a very small range of slopes centered around 0 V/G_0-nm for the 1000, 700, and 650 nm bandpass filters, fitting with the trend observed in Figure S3.

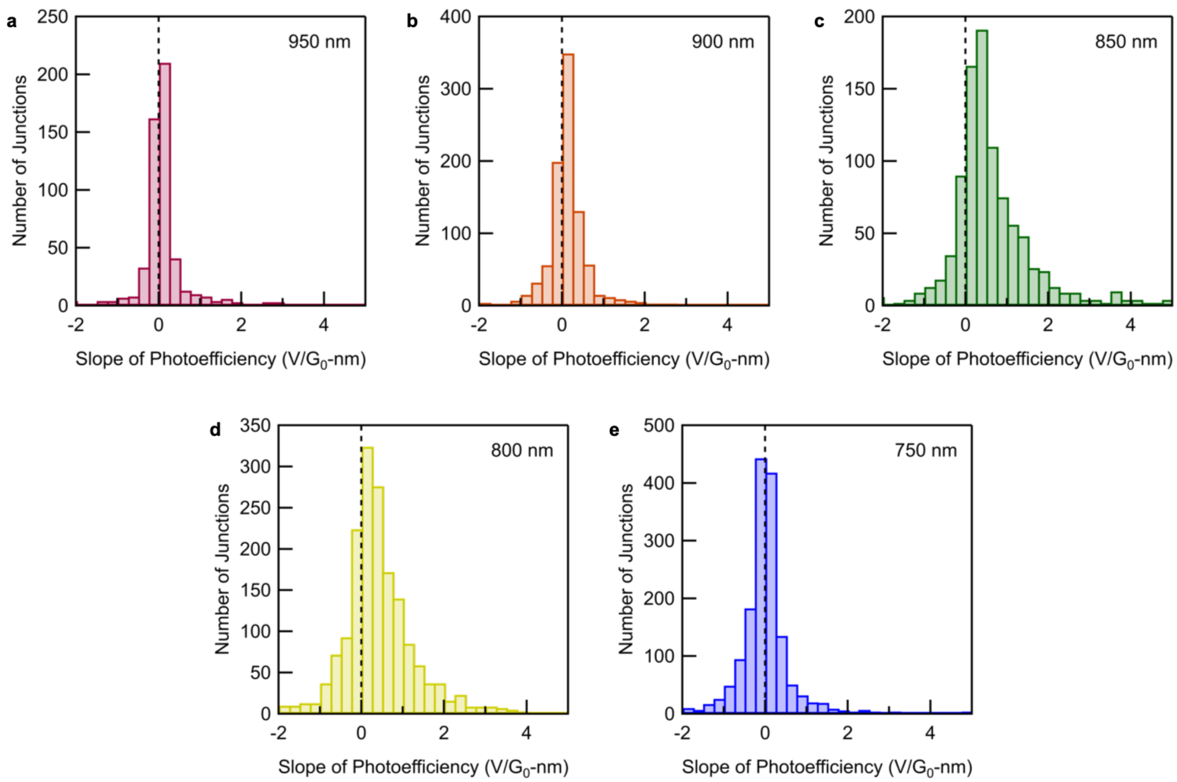

Figure S3. Histogram of photoefficiency slopes for light emission of wavelengths approximately equal to (a) 950 nm, (b) 900 nm, (c) 850 nm, (d) 800 nm, and (e) 750 nm. Each histogram contains 500 to 1800 traces, selected for contact reformation and photovoltage signal above noise.

Finally, we note that the trend seen of increasing photoefficiency with decreasing gap is not due to the wavelength-dependent responsivity of the SiPM. Savage et al. have shown that the plasmonic scattering peak, which indicates the energy of the plasmon resonance, blueshifts in the quantum regime.[4] The SiPM is more sensitive to higher energy photons, but we assert that this is not the main reason for seeing increasing photoefficiency with decreasing gap. We see the same trend even within the small energy range of a 10 nm FWHM bandpass filter when measuring light of approximately 850 or 800 nm. Additionally, we correct our spectra by the detector's responsivity and see that photoefficiency increases as the gap is closed in Figure 3a even after this correction based on the work of Martinenghi et al.[5]

S5. Photoefficiency Trend Depends on Bias

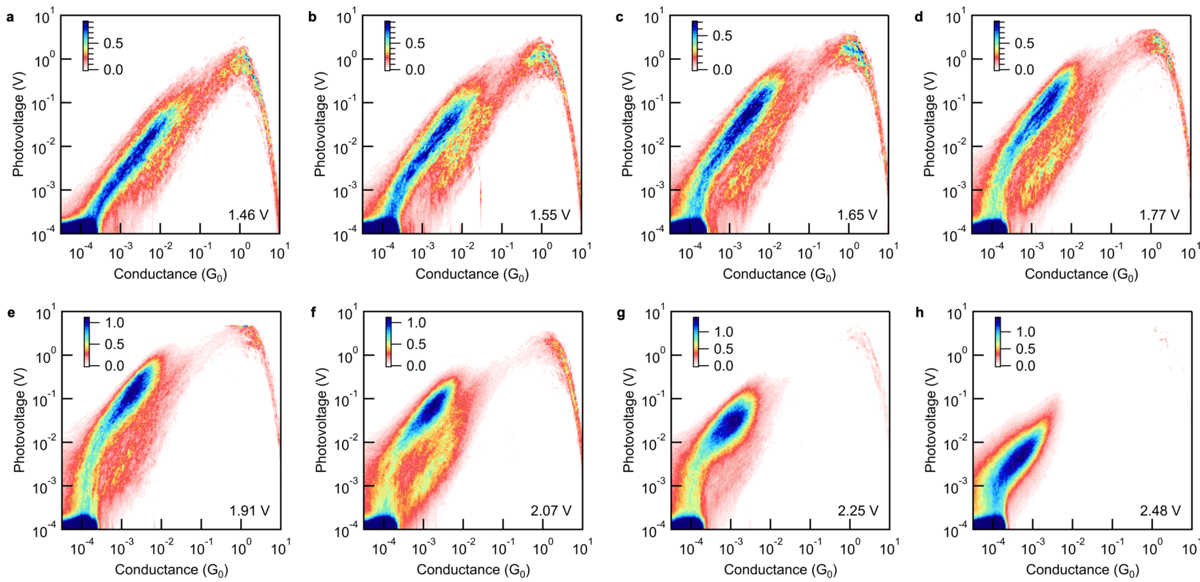

Figure S4. Two-dimensional histogram of photovoltage vs conductance in the applied bias region for biases of (a) 1.46 V, (b) 1.55, (c) 1.65 V, (d) 1.77 V, (e) 1.91 V, (f) 2.07 V, (g) 2.25 V, (h) 2.48 V. Each histogram contains 1400 to 2200 traces.

In Figure S4, we present two-dimensional photovoltage vs. conductance correlation histograms that show the bias dependence to the intensity of light emission. We see that the intensity of the photovoltage for a given conductance (hence, the photoefficiency) increases from 1.46 to 1.91 V, then decreases thereafter. The same tip is used for Figure S4a-e. A second tip is used for Figure S4f-h, but we have confirmed that this second tip gives similar results at 1.65 V to the first tip.

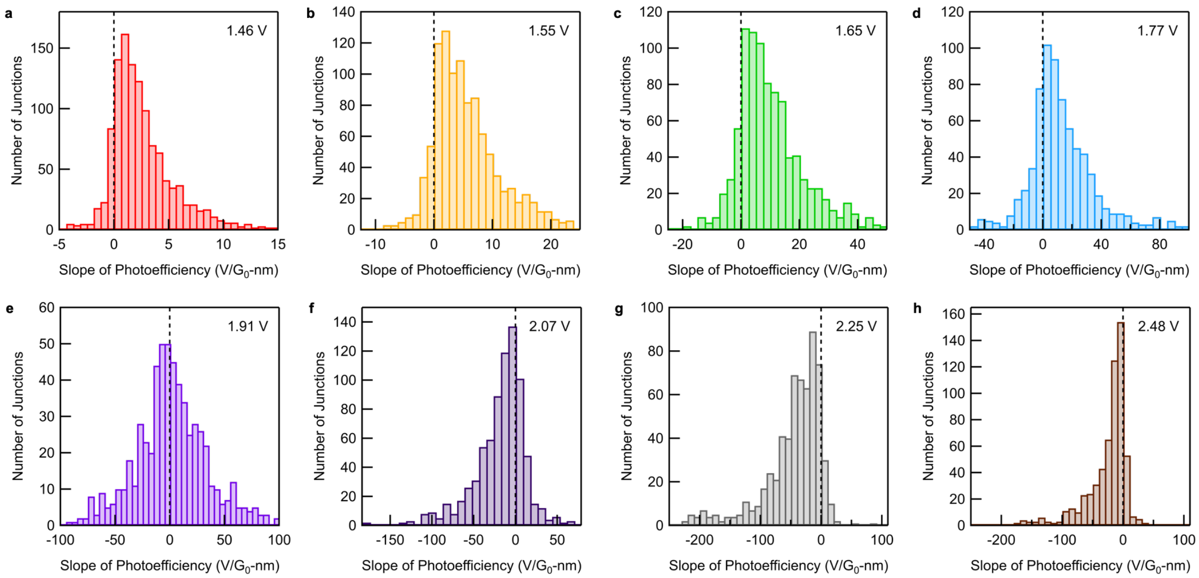

Figure S5. Histograms of photoefficiency slopes for applied biases of (a) 1.46 V, (b) 1.55, (c) 1.65 V, (d) 1.77 V, (e) 1.91 V, (f) 2.07 V, (g) 2.25 V, (h) 2.48 V. Each histogram contains 600 to 1200 traces.

In Figure S5, we show the photoefficiency slope histograms for the same traces that compose the histograms in Figure S4, selecting only traces that reform contact and have a photovoltage signal above noise. As shown in Figure S5, for biases of 1.77 V and below, we see that the majority of traces have a positive slope (increasing photoefficiency as the gap closes). This indicates that plasmonic enhancement of the low energy LSPR increases as the distance between electrodes decreases. At 1.91 V, we see equal proportions of increasing and decreasing photoefficiency as the gap closes and for 2.07 V and higher, we see that the majority of junctions have a strongly negative photoefficiency slope. As discussed in the main text, this trend at high bias likely occurs because of coupling to a plasmonic resonance similar in character to the BDP seen in dimers. The plasmonic enhancement of the BDP has been shown to decrease as the gap between electrodes closes.[6-13] We recognize a slight deviation from this trend at 2.48 V, which has a slightly lower proportion of negatively sloped traces than 2.25 V. One possibility is that the signal to noise ratio is slightly lower at 2.48 V (Figure S4), limiting the slope magnitude. It is also plausible that light emitted from junctions biased at 2.48 V have some degree of coupling to an even higher energy plasmon. Such a plasmon could behave similarly to the bonding quadrupolar plasmon (BQP) seen in dimers, which does not have a gap size-dependent change in plasmonic enhancement.[13]

We also show the wavelength dependence to high bias photoefficiency trend in Figure S6. There are equal positive and negative photoefficiency slopes when measuring light of 850 nm and longer, but the majority of junctions are negatively sloped when measuring light of 650 nm and shorter. Because the higher energy light displays a decrease in photoefficiency as the gap closes, we have further evidence that the plasmon responsible for this change in plasmonic enhancement at higher energies is comparable to the BDP seen in scattering studies of dimers.

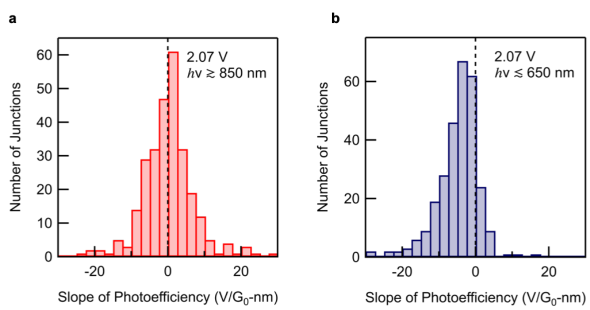

Figure S6. Histogram of photoefficiency slopes for an applied bias of 2.07 V when measuring light of wavelengths (a) 850 nm and longer and (b) 650 nm and shorter. Each histogram contains approximately 300 traces.

S9. Emitted Light is Unpolarized

Figure S7 shows that light emission from the tunnel junctions described in this work is unpolarized. Adding a polarization filter does decrease the overall magnitude of the light emitted, but we observe nearly equal magnitude regardless of the position of the polarizer.

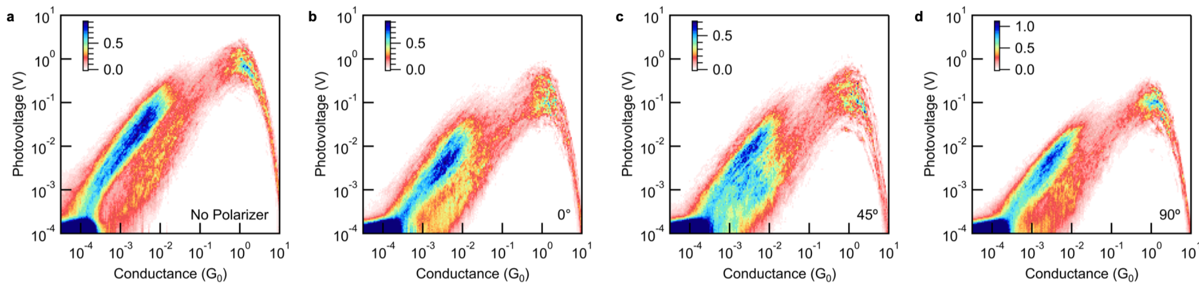

Figure S7. *Two-dimensional histograms of photovoltage vs conductance for (a) all collected light emission, (b) light emission polarized parallel to the applied electric field, (c) light emission polarized 45° to the applied electric field, and (d) light emission polarized perpendicular to the applied electric field. A linear polarizer (Thorlabs) is used. Between 1500 and 2200 traces are represented by each histogram.*

References

1. Tobiska, J.; Danon, J.; Snyman, I.; Nazarov, Y. V. Quantum tunneling detection of two-photon and two-electron processes. *Phys. Rev. Lett.* **2006,** 96 (9), 096801.

2. Xu, F.; Holmqvist, C.; Rastelli, G.; Belzig, W. Dynamical Coulomb blockade theory of plasmon-mediated light emission from a tunnel junction. *Phys. Rev. B.* **2016,** 94 (24).

3. Fung, E. D.; Venkataraman, L. Too Cool for Blackbody Radiation: Overbias Photon Emission in Ambient STM Due to Multielectron Processes. *Nano Lett.* **2020,** 20 (12), 8912-8918.

4. Savage, K. J.; Hawkeye, M. M.; Esteban, R.; Borisov, A. G.; Aizpurua, J.; Baumberg, J. J. Revealing the quantum regime in tunnelling plasmonics. *Nature* **2012,** 491 (7425), 574-7.

5. Martinenghi, E.; Di Sieno, L.; Contini, D.; Sanzaro, M.; Pifferi, A.; Dalla Mora, A. Time-resolved single-photon detection module based on silicon photomultiplier: A novel building block for time-correlated measurement systems. *Rev. Sci. Instrum.* **2016,** 87 (7), 073101.

6. Zuloaga, J.; Prodan, E.; Nordlander, P. Quantum Description of the Plasmon Resonances of a Nanoparticle Dimer. *Nano Lett.* **2009,** 9 (2), 887-891.

7. McMahon, J. M.; Gray, S. K.; Schatz, G. C. Optical properties of nanowire dimers with a spatially nonlocal dielectric function. *Nano Lett.* **2010,** 10 (9), 3473-81.

8. Esteban, R.; Borisov, A. G.; Nordlander, P.; Aizpurua, J. Bridging quantum and classical plasmonics with a quantum-corrected model. *Nat. Commun.* **2012,** 3, 825.

9. Marinica, D. C.; Kazansky, A. K.; Nordlander, P.; Aizpurua, J.; Borisov, A. G. Quantum plasmonics: nonlinear effects in the field enhancement of a plasmonic nanoparticle dimer. *Nano Lett.* **2012,** 12 (3), 1333-9.

10. Li, R. Q.; Hernangomez-Perez, D.; Garcia-Vidal, F. J.; Fernandez-Dominguez, A. I. Transformation Optics Approach to Plasmon-Exciton Strong Coupling in Nanocavities. *Phys. Rev. Lett.* **2016,** 117 (10), 107401.

11. Takeuchi, T.; Yabana, K. Extremely large third-order nonlinear optical effects caused by electron transport in quantum plasmonic metasurfaces with subnanometer gaps. *Sci. Rep.* **2020,** 10 (1), 21270.

12. Kravtsov, V.; Berweger, S.; Atkin, J. M.; Raschke, M. B. Control of plasmon emission and dynamics at the transition from classical to quantum coupling. *Nano Lett.* **2014,** 14 (9), 5270-5.

13. Scholl, J. A.; Garcia-Etxarri, A.; Koh, A. L.; Dionne, J. A. Observation of quantum tunneling between two plasmonic nanoparticles. *Nano Lett.* **2013,** 13 (2), 564-9.